RMetS
Royal Meteorological Society

A polar low observed over the Norwegian Sea on 3–4 March 2008: high-resolution numerical experiments

Ivan Føre[a]* and Thor Erik Nordeng[a,b]
[a]*Department of Geosciences, University of Oslo, Blindern, Oslo, Norway*
[b]*The Norwegian Meteorological Institute, Blindern, Oslo, Norway*

*Correspondence to: I. Føre, University of Oslo, Department of Geosciences, P.O. Box 1047 Blindern, Oslo 0316, Norway.
E-mail: ifore@geo.uio.no

A polar low (PL) observed over the Norwegian Sea by the IPY-THORPEX research aircraft campaign during 3–4 March 2008 was studied by a series of fine-mesh (3 km) experiments using the state-of-the-art Weather Research and Forecasting (WRF) model. The full-physics experiment simulated the PL intensity, baroclinic nature, surface wind speed and track rather well compared to dropsonde observations and satellite images. Two types of sensitivity experiments were designed to analyse the physical properties of the PL. First, physical processes such as condensational heating and sensible and/or latent heat fluxes were switched off throughout the whole simulation. In the second type, these processes were turned off at later times, which minimized the modification of the polar low environment caused by the absence of one or all of them over a long time period, making it suitable to study the direct effect of the physical processes on the PL itself. These two types of sensitivity experiments suggested the following: low-level baroclinic energy conversion was of primary importance for the PL development, while other physical processes had a minor direct impact on the PL intensity. The surface latent heat fluxes, and to a lesser extent sensible heat fluxes, played an indirect role in the sense that they set up and supported the baroclinic environment vital for the PL development. Condensational heating, however, was essential to set up the initial baroclinic environment favourable for the PL intensification, while it had a modest indirect effect thereafter. The experiments indicated that in the late mature stage, after baroclinicity vanished, surface energy fluxes (sensible and/or latent heat) might have contributed to the PL energetics. How the variability in the simulated moist convection, the thermal structure of the PL core, and surface energy fluxes in each experiment affected the PL was difficult to answer.

Key Words: polar lows; condensational heating; surface energy fluxes; IPY-THORPEX

Received 27 July 2011; Revised 21 February 2012; Accepted 27 February 2012; Published online in Wiley Online Library 20 April 2012

Citation: Føre I, Nordeng TE. 2012. A polar low observed over the Norwegian Sea on 3–4 March 2008: high-resolution numerical experiments. *Q. J. R. Meteorol. Soc.* **138**: 1983–1998. DOI:10.1002/qj.1930

1. Introduction

With the goal of improving both weather forecasts and the understanding of severe Arctic weather events such as polar lows, the Norwegian International Polar Year–THe Observing system Research and Predictability EXperiment (IPY-THORPEX) aircraft campaign was launched in February and March 2008 at 69°N, 16°E (Figure 1) in Andenes, Norway (Kristjánsson *et al.*, 2011). Common features of most types of polar low (PL) are that they are short-lived (<48 hours), mesoscale (200–1000 km) cyclones with surface wind speeds above gale force (Rasmussen

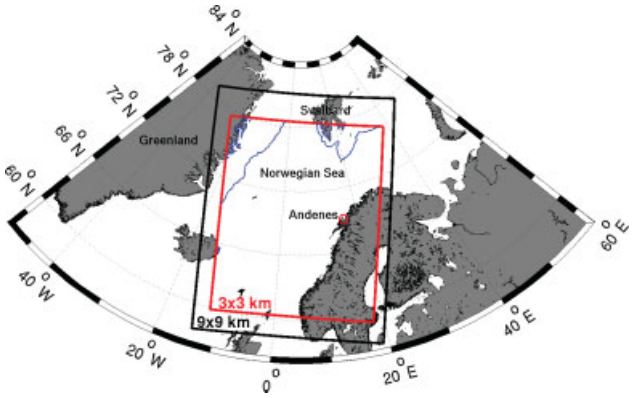

Figure 1. Geographical features and the computational domains. The black square indicates the parent domain (9 × 9 km), and the red square indicates the nested domain (3 × 3 km grid spacing).

and Turner, 2003), and they typically develop during the winter in marine cold air outbreaks (MCAO) (Kolstad, 2006; Kolstad and Bracegirdle, 2008).

A comprehensive study of the three-dimensional structure and underlying physics of the PL based on the dropsonde data from three flight missions, infrared National Oceanic and Atmospheric Administration (NOAA) satellite images, and products from the operational Norwegian High Resolution Limited Area Model (HIRLAM) (Undén *et al.*, 2002) was presented by Føre *et al.* (2011). In short, cross-sections of dropsonde data showed that the horizontal gradients of potential temperature weakened as the PL matured, which suggested that baroclinic energy conversion took place. Dropsonde data on potential temperature and relative humidity showed evidence of a tropopause fold, which is a possible manifestation of an upper-level potential vorticity (PV) anomaly (Hoskins *et al.*, 1985). This was corroborated by a PV inversion, which showed a dominant role for upper-level PV forcing (e.g. Montgomery and Farrell, 1992) throughout the PL's life cycle (Føre *et al.*, 2011). Furthermore, the increased moisture and warming of the planetary boundary layer (PBL) as the PL matured could be related to the increased estimated surface energy fluxes based on dropsonde data and bulk formulae seen in the same period. As Craig and Gray (1996) showed in numerical experiments, surface energy fluxes could be essential for the energetics in some polar low developments. However, it is not easy to understand either the separate roles of condensational heating (i.e. the air is heated from release of latent heat by condensation), surface energy fluxes, and baroclinic energy conversion or their interactions for the PL intensity by using only the dropsonde data and HIRLAM analyses presented in Føre *et al.* (2011).

For this reason, we applied a commonly used method (Mailhot *et al.*, 1996; Bresch *et al.*, 1997; Yanase *et al.*, 2004) in which physical processes were artificially removed during numerical experiments and were compared with a full-physics simulation. Such a method may reveal the role of the physical processes for the PL intensity (section 4). By running the UK Met Office Unified Model (UM), McInnes *et al.* (2011) demonstrated that the decrease of the horizontal grid spacing from 12 to 4 km and then to 1 km significantly improved the simulation of PL development. Indications of the improved model performance at higher resolution were found to be connected to the model's handling of convection. In a numerical experiment where condensational heating was reduced to 10% of its original value, McInnes *et al.* (2011) demonstrated the importance of moist convection and hence condensational heating for the PL energetics. The importance of condensational heating for the intensity of polar lows has been stressed in several previous polar low case-studies (e.g. Sardie and Warner, 1985; Nordeng, 1987; Mailhot *et al.*, 1996; Bresch *et al.*, 1997; Wu and Petty, 2010). Nevertheless, to our knowledge, the role of surface energy fluxes (sensible and/or latent heat) in the PL development has not been analysed to the same degree, and it is therefore the main goal of this study. For comparison with McInnes *et al.* (2011) and previous studies, we also include experiments related to condensational heating and the treatment of moist convection in the model to reveal the PL underlying physics (section 4).

This investigation used high-resolution (3 km mesh) simulations with the full-physics version of the state-of-the-art Weather Research and Forecasting (WRF) model (see section 2). A disadvantage of the commonly performed sensitivity studies (e.g. Craig and Gray, 1996; Bresch *et al.*, 1997; McInnes *et al.*, 2011) is that the various physical properties such as condensational heating and/or surface energy fluxes are turned off throughout the whole integration time. In such experiments it is difficult to judge (Yanase *et al.*, 2004) whether the removal of a certain physical process affects the polar low intensity directly, or indirectly through modification of the environment within which the polar low develops (Føre *et al.*, 2012). In addition to the more commonly used sensitivity experiments, we apply the new type of sensitivity experiment introduced by Yanase *et al.* (2004). Based on these new types of sensitivity experiment, we will discuss which physical process is directly important for the PL intensity and how it affects the PL intensity after the initial and mature environment conditions have been set up (section 4). A summary and discussion is presented in section 5. Before the sensitivity experiments are analysed, section 3 briefly compares the full-physics experiment and the horizontal plots of dropsonde data and satellite images presented in Føre *et al.* (2011). The full-physics simulation was used as a reference run during the analysis of the sensitivity experiments.

2. Model description and experiment design

2.1. *The numerical model*

The WRF model is a mesoscale numerical weather-prediction system used worldwide in operational forecasting and atmospheric research. It integrates the non-hydrostatic, compressible dynamical equations with an Arakawa C-grid using a terrain-following vertical coordinate. This study used version 3.1 of the WRF (Skamarock *et al.*, 2005). The following physical parametrizations were used for the full-physics experiment: the Thompson microphysics scheme (Thompson *et al.*, 2004, 2006); the Betts–Miller–Janjić cumulus scheme (Janjić, 1994, 2000); the Yonsei University planetary boundary layer scheme (Hong *et al.*, 2006); the Noah Land Surface model (Chen and Dudhia, 2001); the MM5 similarity surface scheme (Skamarock *et al.*, 2005); the Rapid Radiative Transfer Model look-up table (Mlawer *et al.*, 1997); and the Dudhia long-wave and short-wave radiation schemes (Dudhia, 1989). The magnitude of the simulated surface energy fluxes is controlled by

roughness length, surface wind speed, relative humidity, and air–sea temperature differences (Chen and Dudhia, 2001). According to Claud *et al.* (2004), the simulated polar low track can be sensitive to the number of vertical levels in the PBL. For this reason, and to increase the resolution of physical processes in the PBL assumed crucial for polar low developments, 18 out of the 60 vertical levels used in this study were set below 850 hPa. Føre *et al.* (2012) showed that differences in the cloud microphysical scheme during the WRF simulations did not change the role of condensational heating for the Barents Sea polar low. For this reason, only the Thompson cloud microphysical scheme was used in this study. All simulations were carried out with positive-definite advection of scalars, moisture, and turbulent kinetic energy.

The WRF model (version 3) was recently applied in a polar low study by Wu *et al.* (2011) in which the National Centers for Environmental Prediction (NCEP) analyses ($1^\circ \times 1^\circ$ latitude–longitude grid) were used as initial and lateral boundary conditions. According to Renfrew *et al.* (2002), NCEP analyses overestimate both wind speed and surface fluxes over the sea, while the European Centre for Medium-range Weather Forecasts (ECMWF) analyses are within the bounds of observational uncertainties. Thus, in our study, we used ECMWF T511 data with $0.5^\circ \times 0.5^\circ$ latitude–longitude horizontal grid resolution with 26 vertical levels as the initial and lateral boundary conditions. It should be mentioned that the ECMWF analyses were improved by the dropsonde observations that were sent in real time to the global telecommunication system (GTS) during the IPY-THORPEX campaign (Irvine *et al.*, 2011).

In Figure 1, the black square shows the 9 km parent domain and the red square the 3 km nested domain. The location of the ice edge and the sea-surface temperature (not shown) were held constant throughout the simulations. McInnes *et al.* (2011) showed that the simulation of the PL was sensitive to the initial conditions and hence the start time of the model runs. Sensitivity experiments (not shown) showed that the WRF model performance was optimal when the simulations were initiated about 36 hours prior to the first signatures of the PL, which is in agreement with the result of the UM simulations presented in McInnes *et al.* (2011). For this reason, all simulations of the PL, apart from those for the delayed (D) experiments, were initialized at 0000 UTC on 2 March and ended at 0000 UTC on 5 March. The role of initial conditions and start time of the WRF simulations in the present study will not be discussed further.

In the present study, the WRF model simulations were carried out with two-way nesting, which was not used (McInnes, personal communication) during the UM model simulations of the PL presented in McInnes *et al.* (2011). When feedback is on, the values of the parent domain (9 km mesh) are overwritten by the values of the variables in the nest (3 km) at the coincident points. This obtains the best possible WRF simulations of the PL, since the boundary conditions for the nested domain come from the parent domain. Both the parent and the nested domain showed more or less identical tracks and are therefore not comparable with the dispersed tracks seen in McInnes *et al.* (2011). Thus, the results from only the 3 km mesh are discussed in this study.

Table 1. A brief summary of the characteristics of each planned model experiment for the polar low.

Abbreviation	Description
CTRL	The default model experiment.
Cu	The convection scheme was turned on throughout the whole simulation only for this. experiment.
NoCH	Condensational heating was turned off throughout the whole simulation.
NoCH-D36	Condensational heating was turned off at 12 UTC on 3 March and the following 30 hours.
NoCH-D48	Condensational heating was turned off at 00 UTC on 4 March and the following 18 hours.
NoF	Surface fluxes of sensible heat and latent heat were turned off throughout the whole. simulation.
NoF-D36	Surface fluxes of sensible heat and latent heat were turned off at 12 UTC on 3 March and the following 30 hours.
NoF-D48	Surface fluxes of sensible heat and latent heat were turned off at 00 UTC on 4 March and the following 18 hours.
NoF+NoCH	Condensational heating as well as sensible and latent heat fluxes were turned off throughout the whole simulation.
NoSHF	The sensible heat flux was turned off over the sea throughout the whole simulation.
NoSHF-D48	The sensible heat flux was turned off over the sea at 00 UTC on 4 March and the following 12 hours.
NoLHF	The latent heat flux was turned off over the sea throughout the whole simulation.
NoLHF-D48	The latent heat flux was turned off over the sea at 00 UTC on 4 March and the following 12 hours.

2.2. *Experiment design*

A series of sensitivity experiments was carried out in order to reveal the underlying physics of the PL development. The experiments are listed in Table 1, and we describe here their main features. Initially, ordinary experiments in which a physical process was turned off throughout the whole simulation were designed. First, the full-physics control (CTRL) experiment as described above was carried out. In order to test the PL sensitivity to the treatment of convective processes in the model, an experiment in which the cumulus scheme was turned on (Cu) for the nested domain was done. In another simulation, the condensational heating was turned off (NoCH), and the role of atmospheric latent heat release was investigated by turning off the heat contribution to the atmospheric temperature profile given by the microphysics schemes after each integration time step. All other processes in the cloud microphysics schemes were carried out normally.

A second group of four experiments was designed to test the PL sensitivity to surface energy fluxes. First, an experiment with no surface energy fluxes (NoF) was carried out. Two similar experiments were then conducted to test the sensitivity to removal of only sensible heat fluxes (NoSHF) or only latent heat fluxes (NoLHF) over the sea. To isolate the role of dry baroclinicity, an experiment with no surface energy (sensible and latent heat) fluxes and no condensational heating was performed (NoF+NoCH).

Following the new type of sensitivity experiment discussed in the introduction, a third group of experiments was designed in which various physical processes (condensational heating and sensible and/or latent heat fluxes) were artificially shut off at later times. This was done by restarting

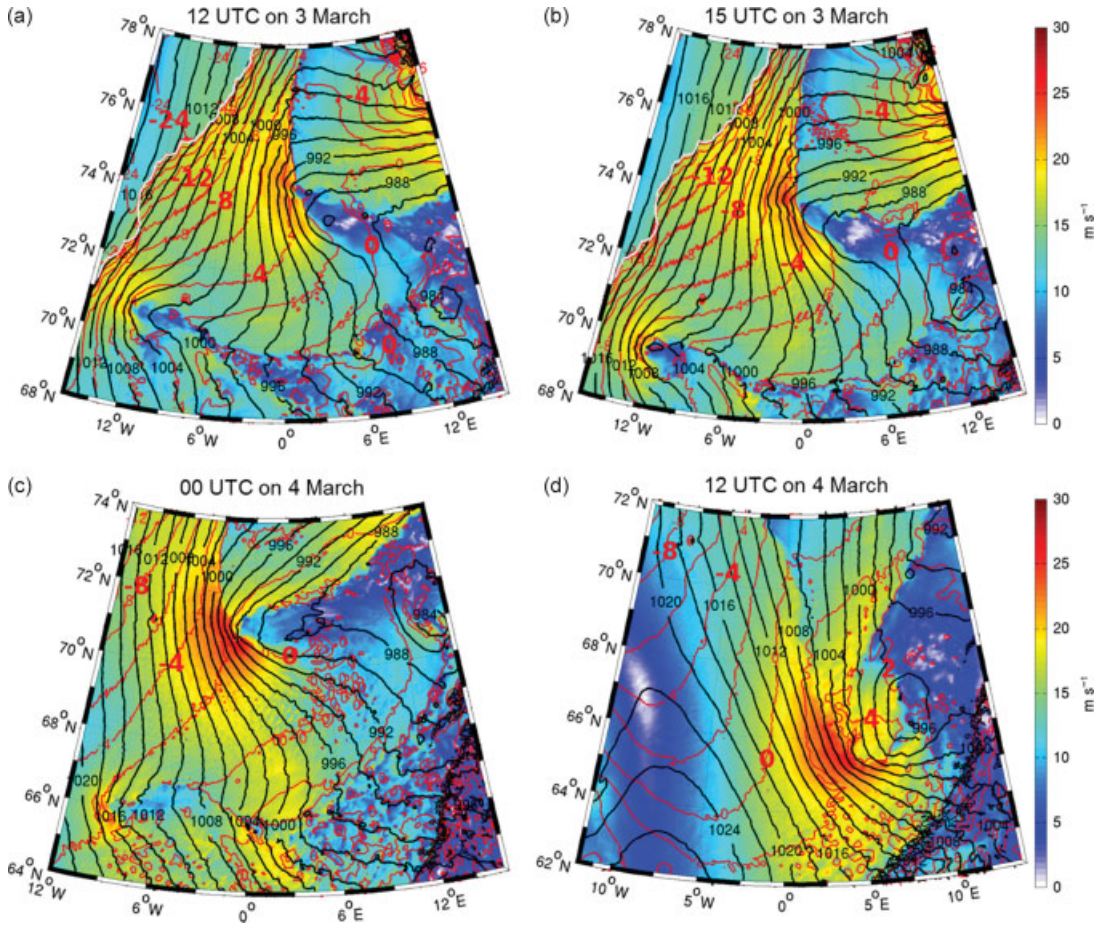

Figure 2. Mean-sea-level pressure (MSLP, hPa, black contours), temperature at 2 m (2°C interval, red contours), and surface wind speed (m s^{-1}, colour shading) in the CTRL experiment. The black arrows show surface wind direction. The sea ice edge is shown by a thick white curve. The times are as follows: (a) 1200 UTC on 3 March, (b) 1500 UTC on 3 March, (c) 0000 UTC on 4 March, and (d) 1200 UTC on 4 March.

the WRF model at different times using the CTRL run as initial conditions. The abbreviations of these experiments end with the capital letter D (delayed) and the numbers 36 or 48, which stand for the number of hours into the integration CTRL was run before specific physical processes were turned off. In the -D36 experiments, the physical processes were turned off throughout the PL lifetime, which was from 1200 UTC on 3 March until 1800 UTC on 4 March. In the -D48 experiments, they were turned off at 0000 UTC on 4 March for the following 18 hours. However, the NoLHF-D48 and NoSHF-D48 were terminated at 1200 UTC on 4 March. According to Yanase *et al.* (2004), if a physical process had a 'direct effect' on the vortex itself, a decrease in the polar low intensity would be observed within 1–3 hours. Any reduction in the polar low intensity thereafter could also be related to the deformation of the polar low environment, which is hereafter referred to as the 'indirect effect'. Thus, the direct effect is determined by comparing the CTRL with each delayed (D) experiment, 3 hours after the delayed experiments were initiated.

3. Evolution of the polar low in the CTRL experiment

In this subsection, the CTRL experiment is analysed. In the aftermath of a synoptic low that moved eastward across the Norwegian Sea on early 2 March 2008, two well-defined convergence zones developed between Greenland and Svalbard on 3 March 2008 (Føre *et al.*, 2011).

At 1200 UTC on 3 March, during the first flight mission on 3 March (Føre *et al.*, 2011), the high vertical velocities and the gradients of surface wind speed showed the approximate surface position of a north–south oriented convergence zone seen along the 0°E meridian, stretching from the sea ice edge at about 78°N to about 74°N (Figure 2(a)). The 500–1000 hPa thickness showed the baroclinic structure of the zone (Figure 3(a)), and as demonstrated by the 2 m temperature, an outbreak of Arctic air took place on its western side (Figure 2(a)). Similar to the arguments above, a second convergence zone was seen along the 73°N latitude stretching from the 2°E meridian eastward (Figures 2(a) and 3(a)) which, according to the 500–1000 hPa thickness, had cold air masses on both sides. It should be mentioned that the baroclinic zone was mostly confined below the 700 hPa level, in good agreement with dropsonde observations (Føre *et al.*, 2011). This warm tongue of air was created by relatively cold northwesterly winds north of the zone and the warmer and calmer air masses to its south. The above observations are in good agreement with the dropsonde and satellite observations presented in Føre *et al.* (2011). According to the satellite images, the PL developed close to the intersection between the two convergence zones during the following 12 hours (Føre *et al.*, 2011). Based on the mean-sea-level pressure (MSLP) (986 hPa), the CTRL simulated the initial stage of the PL (73°N, 5°E) about 2° too far to the west (Figure 2(a)) according to dropsonde observations (Føre *et al.*, 2011).

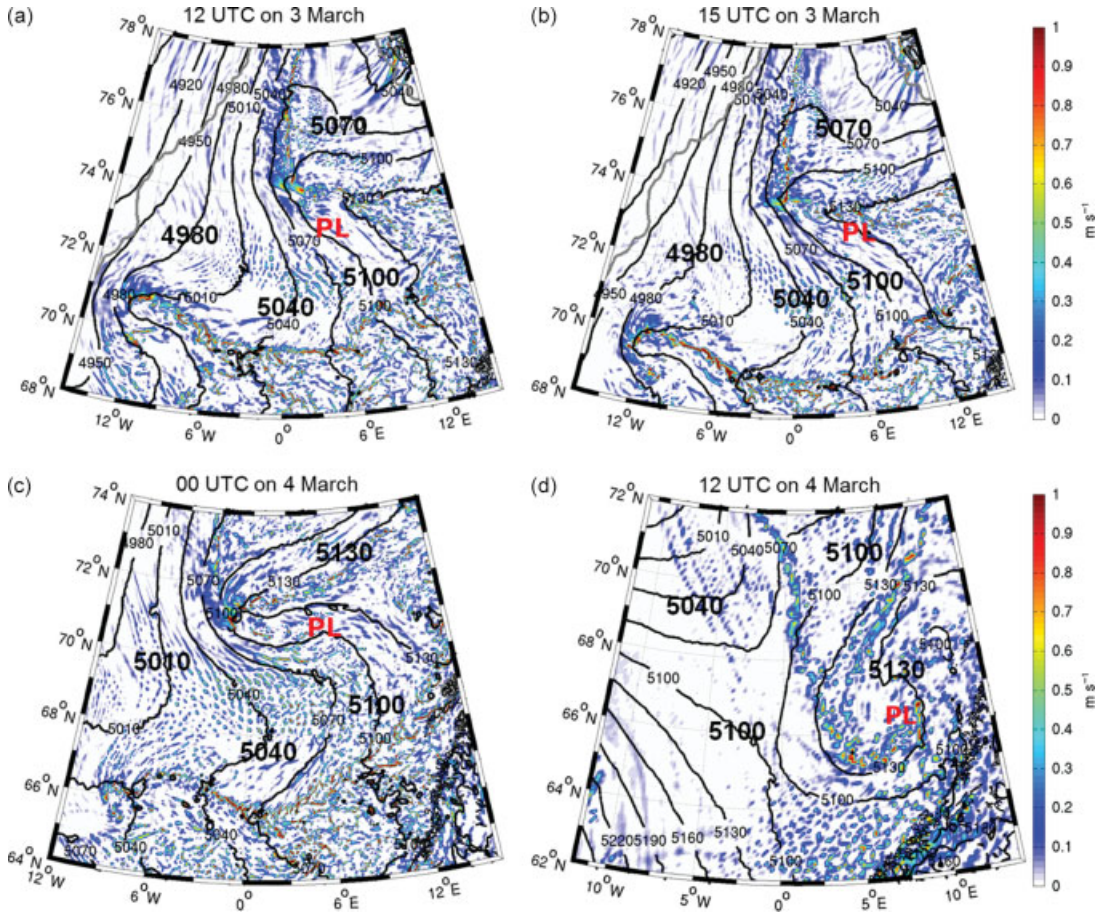

Figure 3. Vertical wind speed (m s^{-1}, colour shading) at 850 hPa surface and 500–1000 hPa thickness (30 m interval, black contours) in the CTRL experiment. The sea ice edge is shown by a thick grey curve. The times are as follows: (a) 1200 UTC on 3 March, (b) 1500 UTC on 3 March, (c) 0000 UTC on 4 March, and (d) 1200 UTC on 4 March. The red capital letters (PL) indicate the approximate central position of the simulated PL shown in Figure 2.

However, the simulated maximum surface wind speed was about 2 m s^{-1} weaker according to observations (not shown). Further downwind, more or less parallel to the 70°N latitude, between 12°W and 6°E, the high vertical velocity and gradients of surface wind speed showed another convergence zone (Figures 3(a) and 2(a), respectively), which will hereafter be referred to as an Arctic front. The Arctic front was clearly visible in the satellite images, at roughly the same location (Føre *et al.*, 2011). Both the 2 m temperature (Figure 2(a)) and the 500–1000 hPa thickness (Figure 3(a)) showed that the Arctic front had cold air masses on both sides.

According to estimated surface fluxes from the first flight mission on 3 March (Føre *et al.*, 2011), the maximum sensible (320 W m^{-2}) and latent heat (250 W m^{-2}) fluxes south and west of the PL (Figure 4(a) vs. 4(b), respectively) appear to be overestimated by about 50 and 120 W m^{-2}, respectively. Still, the overall simulated latent heat and sensible heat structure fits relatively well with dropsonde observations. Further west and close to the sea ice, the cold air outbreak and strong surface wind speed (Figure 2(a)) triggered maximum sensible and latent heat fluxes of about 600 W m^{-2} and 300 W m^{-2}, respectively (Figure 4(a) vs. (b), respectively). These fluxes cannot be validated since the dropsonde observations did not cover this area (Føre *et al.*, 2011). Nevertheless, these values are relatively modest as compared to previous simulated surface energy fluxes close to the sea ice edge (Bresch *et al.*, 1997; Føre *et al.*, 2012), most likely because of lower surface wind speed (not shown).

At 1500 UTC on 3 March, midway into the second flight mission (Føre *et al.*, 2011), the maximum surface wind speed west of the PL increased to about 25 m s^{-1} (Figure 2(b)). Closer inspection of Figure 2(a) and (b) reveals that, during the preceding three hours, the surface wind speed showed a slightly more cyclonic motion. Therefore, we suggest that the cyclogenesis stage of the simulated PL was initiated at this time, which is in agreement with the observed PL (Føre *et al.*, 2011).

At about 0000 UTC on 4 March, the simulated PL (988 hPa) reached its mature stage with a maximum surface wind speed of about 26 m s^{-1} on its cold western side (~71° N, 6°E; Figure 2(c)). The evolution of the 2 m temperature (Figure 2(b)–(c)) and 500–1000 hPa thickness (Figure 3(b)–(c)) shows that as the MCAO wrapped around the simulated PL on its southern side, it was warmed by surface energy fluxes. While this took place, the warm tongue discussed above moved southeastward (Figure 3(b)–(c)). The high vertical velocities west of the PL as this took place (Figure 3(b)–(c)) imply that the warm tongue ascended over the MCAO, and this is a manifestation of the baroclinic energy conversion that took place during the PL development. It should be mentioned that the warm tongue was an important factor in the discussion of the sensitivity experiments (see section 4). The Arctic front, with structures similar to those discussed above, moved southeastward and was now off the coast of Norway, curving westward along the 66°N latitude to about 6°W (Figure 2(c)), where it turned northward to about 70°N, which is in good agreement with

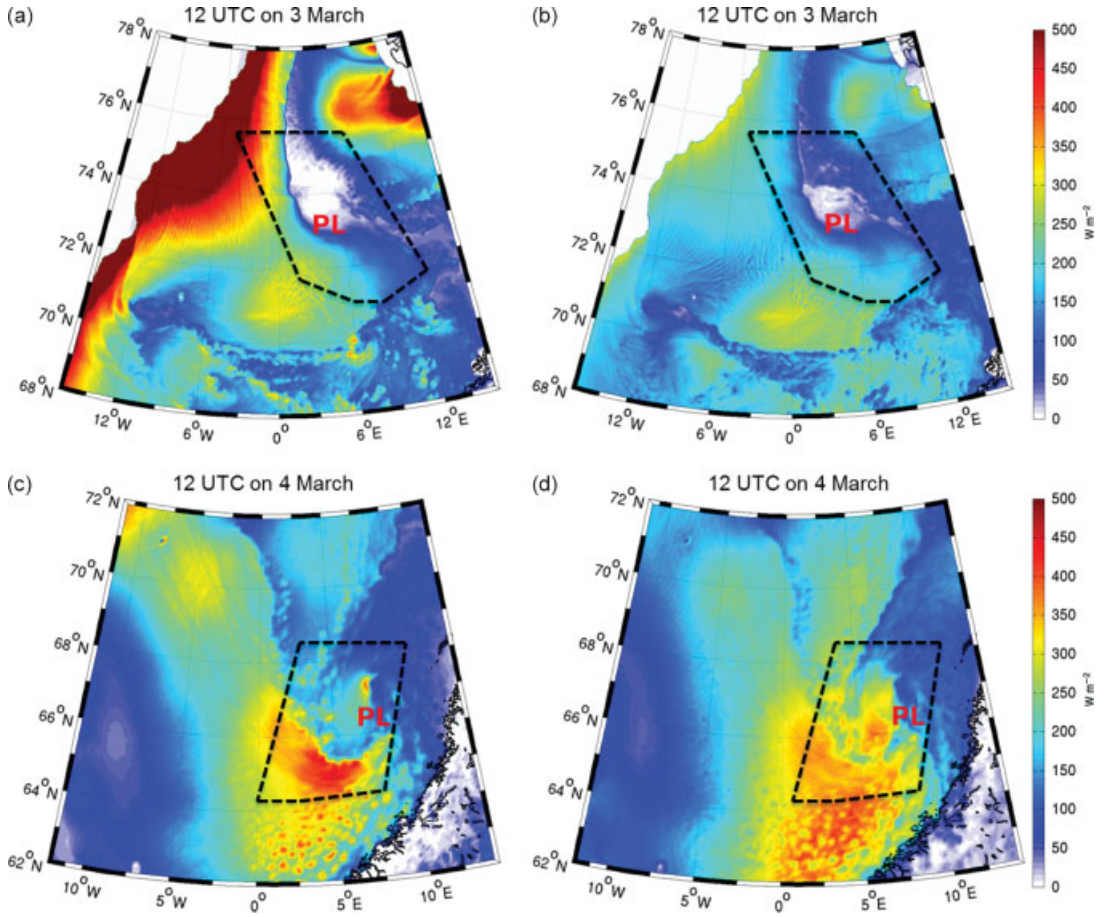

Figure 4. Surface sensible heat (left column) and latent heat (right column) fluxes (W m^{-2}) in the CTRL experiment. The sea ice and land masses are shown as areas of almost zero fluxes. The times are as follows: (a), (b) 1200 UTC on 3 March 2008, the dashed black lines show the approximate area of estimated surface fluxes from the first flight mission; (c), (d) 1200 UTC on 4 March, the dashed black lines show approximately the area of estimated surface fluxes during the third flight mission. The red capital letters (PL) indicate the approximate central position of the simulated PL shown in Figure 2.

the satellite images presented in Føre *et al.* (2011). The cross-section of PV shows evidence of a phase lock between an eastward-moving upper-level PV anomaly (not shown) and the PL, which is in agreement with the PV scenarios described in Føre *et al.* (2011). The role of upper-level PV forcing is not within the scope of this study and therefore is not discussed further.

During the following 12 hours, the PL moved southeastward as it weakened. At 1200 UTC on 4 March, during the third flight mission that observed the mature stage of the PL (Føre *et al.*, 2011), the CTRL (Figure 2(d)) simulated the PL (994 hPa) about 1° too far southeast (67°N, 8°E) according to dropsonde observations (Føre *et al.*, 2011). The maximum surface wind speed increased to approximately 26–27 m s^{-1}, although the simulated PL had weakened by 10 hPa during the preceding 24 hours (Figure 2(a) vs. 2(d), respectively). This increase in surface wind speed was caused by sharpened pressure gradients on the southwestern side of the PL, which is in good agreement with dropsonde observations (Føre *et al.*, 2011). By then, maximum sensible and latent heat fluxes southwest of the PL were about 450 W m^{-2} and 400 W m^{-2}, respectively. Both surface energy fluxes were overestimated by about 150 and 100 W m^{-2}, respectively, according to the estimated surface fluxes presented in Føre *et al.* (2011). Similar to the observed PL (Føre *et al.*, 2011), the CTRL simulated a warm-core PL, which, at surface levels, was about 4°C warmer than the cold air on its southwestern side (Figure 2(d)). As demonstrated by the 500–1000 hPa thickness evolution (Figure 3(c)–(d)) as the PL matured, the warm tongue had wrapped around the PL as it moved into a less baroclinic and warmer environment. Thus, warm air seclusion could explain the warm-core PL. The high vertical velocities at the central structure of the simulated PL (Figure 3(c)–(d)) suggest that moist convection followed by condensational heating may have contributed to the energetics of the PL, in agreement with the observed high values (70%) of relatively humidity up to the tropopause (Føre *et al.*, 2011). Further, the increased surface energy fluxes could also contribute to the PL energetics (Craig and Gray, 1996). The plots of 500–1000 hPa thickness showed that baroclinicity vanished after 1200 UTC on 4 March (not shown), implying that a forcing mechanism other than low-level baroclinic energy conversion contributed to the PL energetics. Similar to the satellite images, at about 1800 UTC the same day, the simulated PL made landfall over the coast of Norway at about 64.5° N, 11° E.

We believe that the simulated surface fluxes presented in this study show a more realistic re-production of the actual surface energy fluxes that took place during the PL development than the estimated surface energy fluxes based on bulk formulae and dropsonde data presented in Føre *et al.* (2011). Based on the above discussion, we conclude that the CTRL run simulates the PL development quite well according to the dropsonde observations and satellite images (Føre *et al.*, 2011), and we therefore conclude

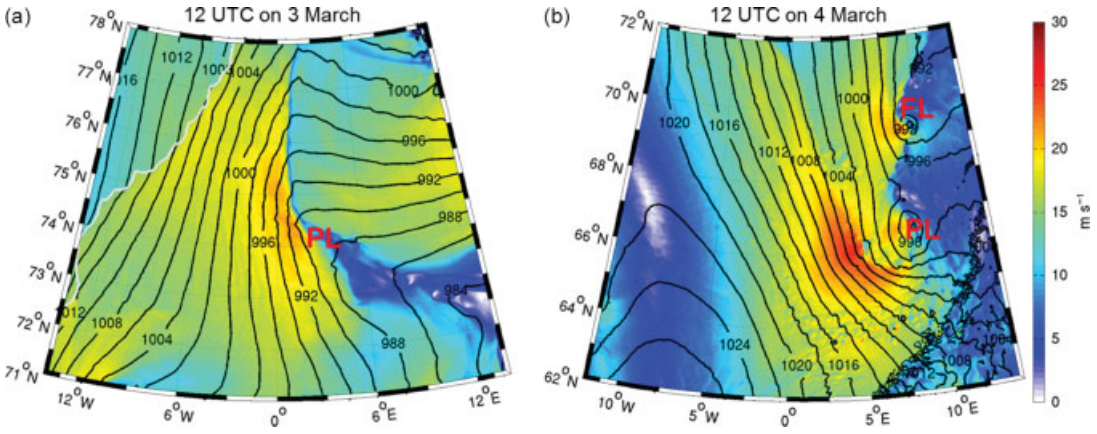

Figure 5. Mean-sea-level pressure (MSLP, hPa, black contours) and surface wind speed (m s^{-1}, colour shading) in the Cu experiment for the following times: (a) 1200 UTC on 3 March, and (b) 1200 UTC on 4 March, 2008. The sea ice edge is shown by a thick white curve. The red capital letters PL and FL show the approximate central position of the simulated PL and the 'false low', respectively.

that the simulated PL is representative of the observed system.

4. Results of the sensitivity experiments

In this section, the PL intensity sensitivity to sensible and latent heat fluxes and their combined effect in addition to condensational heating are investigated (Table 1) in order to clarify the underlying physical processes of the PL development. As demonstrated by the CTRL (Figure 2), the PL intensity weakened, but because of sharpened pressure gradients on its western side, surface wind speed increased in this area as the PL matured. Thus, in order to analyse the PL sensitivity to the various physical processes, we compare plots of MSLP and surface wind speed at various times (see below) using the CTRL as references. This analysis is supplemented by Table 2, which shows a three-hour time evolution of the PL simulated minimum MSLP from each experiment listed in Table 1. The track ends at the final integration time (i.e. NoSHF-D48 and NoLHF-D48), at the time the PL made landfall in each experiment (i.e. CTRL, Cu, NoCH-D36, NoCH-D48 and NoSHF), or at the time the PL died away (No PL, i.e. NoF, NoF+NoCH, NoF-D36, NoF-D48 and NoLHF). In some experiments, the MSLP showed the central position of the PL as a trough rather than with closed isobars (MSLP), especially during early stages of the PL life cycle. In these experiments, the PL position, and hence its minimum MSLP, was decided by combining the position of the trough and the maximum wind speed seen west of the trough. Thus, in some of the simulations (i.e. Cu, NoCH, NoCH-D36, NoF-D36 and NoLHF), the minimum MSLP and position of the PL are somewhat less precise than as seen in the CTRL. It should be mentioned that the continuous decrease in the PL intensity throughout its life cycle, which is not typical for polar lows in that most polar lows show a deepening stage followed by a decrease or maintenance in intensity (Rasmussen and Turner, 2003), made it difficult to separate the direct and indirect effect of the physical processes on the PL intensity. For simplicity, we divided the PL life cycle into three stages based on the CTRL run (Figure 2): the initial stage (at 1200 UTC on 3 March), the cyclogenesis stage (from 1500 UTC to 2100 UTC on 3 March), and the mature stage (from 0000 UTC on 4 March up to PL landfall). These stages will be used in describing the role of the physical processes during the PL life cycle.

Table 3 presents a brief summary of the effects of the various physical processes on polar low intensity based on the result of each sensitivity experiment described in section 2 (Table 1).

4.1. *The role of condensational heating*

As demonstrated by McInnes *et al.* (2011) using the UM model, moist convection could be essential for the observed PL development. Thus, the treatment of convection in the WRF could be crucial in order to reproduce the PL development. For this purpose, we first present a short analysis of the treatment of cumulus convection in the model.

4.1.1. *The treatment of moist convection*

When the cumulus scheme (Cu) was turned on, the model failed to reproduce closed isobars at the area where the PL (988 hPa) developed (74°N, 3°E), and its initial position was simulated about 1.5° too far northwest according to the CTRL run (Figure 5(a) vs. 2(a), respectively). The weaker PL resulted in a 2–3 m s^{-1} reduction in maximum surface wind speed west of the PL. During the cyclogenesis stage, the Cu gave a 1–2 hPa weaker PL (Table 2). As the PL reached the mature stage and up to the time of landfall, Cu showed similar or 1 hPa differences in intensity as compared to the CTRL (Table 2). At 1200 UTC on 4 March, the Cu showed a 994 hPa PL, which is 1 hPa deeper than in the CTRL (Table 2). Also, in the Cu, the PL (67°N, 9°E) was positioned about 1° farther east, and according to the MSLP (996 hPa), the PL central surface structure was too small (Figure 5(b) vs. 2(d), respectively). Furthermore, in the Cu, a 990 hPa deep 'false' low (FL) was seen at approximately 70°N, 10°E, which, in the CTRL run, was hardly visible (Figure 5(b) vs. 2(d), respectively). Additionally, the PL made landfall about three hours too early in the Cu (not shown). Based on the above observations, we conclude that the simulation of the PL and its surrounding environment were improved by explicitly resolving cumulus convection (e.g. CTRL). Thus, in the present study, all experiments were carried out with the cumulus scheme turned off for the nested domain (3 km mesh), which was also the case during the 4 and 1 km mesh PL simulations presented in McInnes *et al.* (2011). During the Pacific polar low case in Sardie and Warner (1985), the

Table 2. A three-hour time evolution (hour and date) of minimum mean-sea-level pressure (MSLP, hPa) for the experiments listed in Table 1. The track starts at 1200 UTC on 3 March 2008, and ends as the PL made landfall or died away (No PL). 'No PL' means that the simulation did not reproduce the PL or that the PL died away at this time.

	12_03	15_03	18_03	21_03	00_04	03_04	06_04	09_04	12_04	15_04	18_04
CTRL	986	987	988	988	988	989	990	991	995	997	1001
Cu	2	2	1	1	1	0	0	1	−1	0	0
NoCH	6	6	5	7	8	9	9	11	10		
NoCH-D36		1	0	1	2	2	2	4	2	4	
NoCH-D48						0	1	3	2	2	2
NoF	No PL										
NoF+NoCH	NoPL										
NoF-D36		0	1	3	5	6	8	11	12	No PL	
NoF-D48						0	1	5	5	7	No PL
NoSHF	2	2	2	3	3	4	5	6	6	8	
NoSHF-D48						0	1	3	2		
NoLHF	3	4	4	4	5	7	9	No PL			
NoLHF-D48						0	0	3	2		
FL_NoCH	2	3	3	4	4	5	4	4	3		
FL_NoLHF	1	0	1	0	1	1	1	3	1		

use of convective parametrization improved the simulation of the polar low, while the opposite (moist convection treated explicitly) was best for the Atlantic case. Thus, the importance of the treatment of moist convection may vary from case to case, making it difficult to assess the typicality of the present model's configuration.

4.1.2. *The role of condensational heating*

Now, let us look at the role of condensational heating (NoCH) for the PL development. At 1200 UTC on 3 March, the NoCH showed that the PL (72.5° N, 6°E) initial stage was largely suppressed by the absence of condensational heating causing a weaker PL by 6 hPa, which, as compared to the CTRL, is simulated about 1° too far southeast (Figure 6(a) vs. 2(a), respectively). Thus, condensational heating seemed to be important to simulate the initial stage of the PL. West of the PL, the NoCH showed weaker pressure gradients, explaining the lower maximum surface wind speed (approximately 5 m s^{-1}). During the cyclogenesis stage, the absence of condensational heating (NoCH) resulted in a 5–7 hPa weaker PL as compared to the CTRL (Table 2). As the PL matured, condensational heating was crucial for the PL development, in that the PL gradually weakened by 8 to 11 hPa as compared to the CTRL (Table 2) and nearly died away. As seen in Figure 6(b), the remnant of the PL (1004 hPa) made landfall (64°N, 11°E) about 6 hours too early according to the CTRL (Figure 2(d)), which shows that the absence of condensational heating caused the PL to move faster southeastward into the less baroclinic and warmer environment (not shown) as it matured. A 'false' low (FL), which was initiated 4° further east of the PL at about 1800 UTC on 3 March (not shown), made landfall several hundred km further north at 69°N, 14°E (Figure 6(b)). Based on the discussion above, it would have been reasonable to suggest that condensational heating was essential for the PL itself, as McInnes *et al.* (2011) suggested based on a similar experiment as the NoCH. However, as will be shown below, condensational heating may not crucial for the PL itself. It should be mentioned that in McInnes *et al.* (2011) the PL showed a similar track and lifetime as the FL discussed above. However, analyses of the FL showed a similar drastic reduction in intensity (not shown) as the PL and thus do not change our suggestion about the role of condensational heating in the NoCH.

To reveal the direct effect of condensational heating on the PL itself we compared the NoCH-D36 and CTRL at 1500 UTC on 3 March. As Figure 7(b) shows, the NoCH-D36 simulated a 1 hPa weaker PL compared to the CTRL (Figure 7(a)). This suggests that condensational heating had a direct effect on the PL intensity during the cyclogenesis stage, after the initial environment conditions were set up (Figure 3(a)). But, it is not until the mature stage that a modest reduction in intensity of 2 to 4 hPa was seen as compared to the CTRL (Table 2). The above observations suggest the following: condensational heating was essential to set up the initial environment of the PL, while it had a modest indirect role on its intensity thereafter. Furthermore, as in the NoCH, the PL moved faster southeastward as it matured, which resulted in landfall about 3 hours too early (Table 2) as compared to the CTRL.

Surprisingly, by comparing the NoCH-D48 with the CTRL at 0300 UTC on 4 March, the condensational heating seemed to have no direct effect on the mature PL (Figure 8(b) vs. 8(a), respectively) because both experiments showed similar PL intensity. Nevertheless, as demonstrated by the MSLP, the central structure of the PL was somewhat affected, and the maximum surface wind speed was reduced about 2–3 m s^{-1}, which implies that condensational heating had some direct effect on the PL. As the PL matured, a 1 to 3 hPa weaker PL was simulated (Table 2) suggesting a modest indirect role of condensational heating, in good agreement with the NoCH-D36. The above observations clearly demonstrate that the new delayed (D) experiments may lead to a different understanding of how condensational heating affects the PL development. The indirect effect

Table 3. Summary of the main results from each experiment.

Abbreviation	Description
CTRL	The PL developed as a result of low-level baroclinic instability interacting with an upper-level PV anomaly.
Cu	Cumulus convection should be treated explicitly.
NoCH	Condensational heating was essential during the initial and cyclogenesis stages while becoming crucially as the PL matured in that the PL nearly died away.
NoCH-D36	Condensational heating had a small direct effect on the PL intensity after the initial environmental conditions were set up, while it had a modest indirect role as the PL matured.
NoCH-D48	Condensational heating had most likely a minor direct effect on the PL intensity after the mature environmental conditions were set up, while it had a modest indirect role thereafter.
NoF	Surface energy fluxes were essential in order to set up the initial low-level baroclinic environment crucially for the PL to develop within.
NoF+NoCH	Surface energy fluxes and condensational heating were essential in order to set up the initial low-level baroclinic environment crucially for the PL to develop within.
NoF-D36	Surface energy fluxes had most likely a minor direct role on the PL intensity after the initial environmental conditions were set up, while it had a crucial indirect role as the PL matured in that it died away.
NoF-D48	Surface energy fluxes had most likely a minor direct role on the PL intensity after the mature environmental conditions were set up, while it had a crucial indirect role as the PL matured in that it died away.
NoSHF	Sensible heat fluxes played a modest role in the initial and cyclogenesis stages while it played a moderate role thereafter.
NoSHF-D48	Sensible heat fluxes had most likely a minor direct on the PL intensity after the mature environmental conditions were set up, while it had a modest indirect role thereafter.
NoLHF	Latent heat fluxes played a dominant role in the initial and cyclogenesis stages, while it had a crucial role thereafter in that the PL died away.
NoLHF-D48	Latent heat fluxes had a minor direct effect on the PL intensity after the mature environmental conditions were set up, while it had a modest indirect role thereafter.

of condensational heating by modification of the PL environment is discussed in subsection 4.3.

4.2. *The role of surface fluxes*

In this subsection, the role of surface sensible (NoSHF and NoSHF-D48) and latent heat (NoLHF and NoLHF-D48) fluxes and their combined (NoF, NoF-D36, NoF-D48) effect in addition to the role of condensational heating (NoF+NoCH) are investigated for the PL development, using the sensitivity experiments described in section 2 (Table 1).

4.2.1. *Both sensible and latent heat fluxes*

The NoF and NoF+NoCH experiments suggest a crucial role of surface energy fluxes for the PL development in that the PL failed to develop (not shown). During the Hudson Bay case in Albright *et al.* (1995) and the Bering Sea case in Bresch *et al.* (1997), polar lows also failed to develop in the absence of surface energy fluxes throughout the whole simulations. In their studies, the polar low developed in a baroclinic zone that was confined to lower atmospheric levels, which are affected by the absence of surface energy fluxes. Bresch *et al.* (1997) argued that by turning off the low-level heating by surface energy fluxes, the lower atmosphere became too stable for the upper-level PV anomaly to penetrate to surface levels (Hoskins *et al.*, 1985), which prevented the formation of the Bering Sea polar low. However, in our case, in the NoF and NoF+NoCH we found evidence that as the eastward-moving upper-level PV anomaly (not shown) moved over the initial area of the observed PL, it initiated circulation at surface levels about 7° east of the observed PL (not shown). Thus, in both the NoF and NoF+NoCH, a false low developed further east of the PL, which made landfall several hundred km further north (not shown) than the observed PL. A likely explanation for the failure to simulate the PL in the NoF and NoF+NoCH is that the low-level heating by surface energy (sensible and latent heat) fluxes was essential in order to set up the initial environment favourable for PL formation, since the warm tongue (i.e. east–west oriented convergence zone) seen along the 73°N latitude east of 0°E in the CTRL (Figures 2(a) and 3(a)) was not successfully simulated in those experiments (not shown). As described above, this warm tongue was essential to the baroclinic nature of the PL development, in that it was wrapped around the PL as it matured.

Surprisingly, the NoF-D36 experiment suggested that surface energy fluxes played a minor direct role for the PL intensity. At 1500 UTC on 3 March, the NoF-D36 and the CTRL showed similar PL (987 hPa) intensity (Figure 7(c) vs. 7(a), respectively). As demonstrated by the MSLP and surface wind speed, the central structure of the PL was somewhat affected which implied some small direct influence of surface energy fluxes on the PL. An important observation is that the surrounding PL environment showed the largest reduction in surface wind speed, which in turn weakened surface energy fluxes and weakened the moist convection throughout (not shown). As the PL matured, however, the NoF-D36 showed the crucial indirect role of surface energy fluxes for the PL intensity, in that the PL gradually weakened up to 12 hPa (Table 2) and died away (not shown). As this took place, the PL environment was gradually deformed and smoothed out (not shown). It is believed that the gradual deformation of the PL environment would lead to the strong reduction in the PL intensity (Table 2). This will be addressed in the subsection below.

An additional experiment (NoF-D48) was designed in order to understand the direct role of surface energy fluxes after the mature PL environmental conditions had been set up. At 0300 UTC on 4 March, the NoF-D48 and the CTRL showed similar intensity (Figure 8(c) vs. 8(a), respectively), which implies that surface energy fluxes (not shown) did not have a direct effect on the mature PL (Table 2). However, as compared to the CTRL, the slightly different MSLP and surface wind speed at the central structure of the PL suggest (Figure 8(c) vs. 8(a), respectively) some small direct influence of surface fluxes. As in the NoF-D36, the PL gradual weakened in the NoCH-D48 (1 to 7 hPa) and died away as it matured (Table 2). Thus, surface energy fluxes

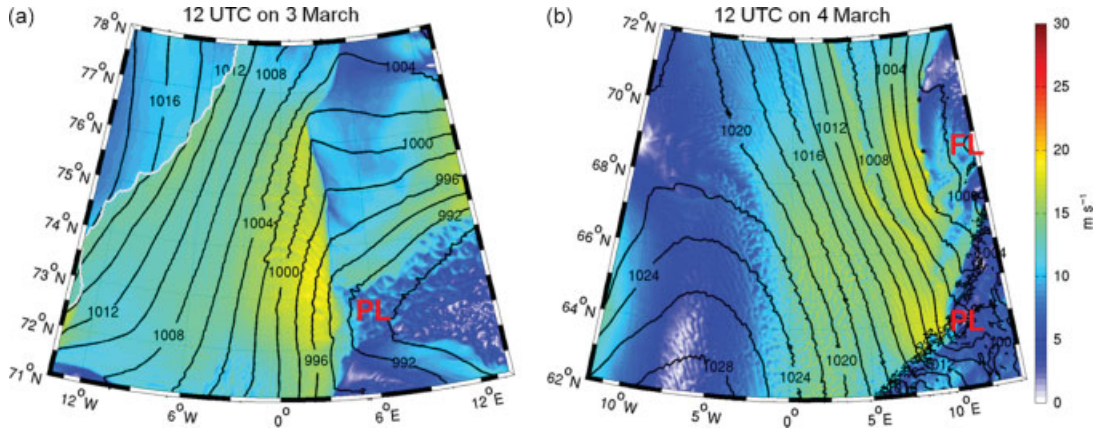

Figure 6. Mean-sea-level pressure (MSLP, hPa, black contours) and surface wind speed (m s^{-1}, colour shading) in the NoCH experiment for the following times: (a) 1200 UTC on 3 March, and (b) 1200 UTC on 4 March, 2008. The sea ice edge is shown by a thick white curve. The red capital letters PL and FL show the approximate central position of the simulated PL and the 'false low', respectively.

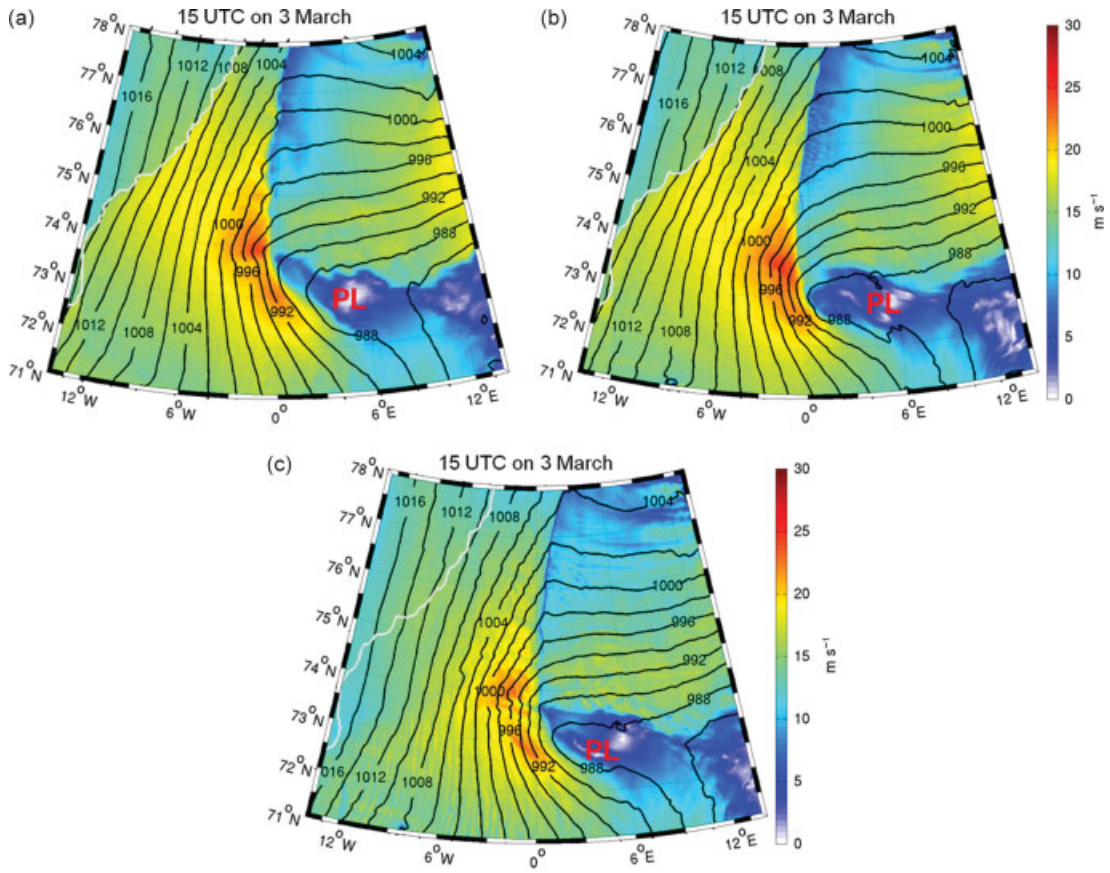

Figure 7. Mean-sea-level pressure (MSLP, hPa, black contours) and surface wind speed (m s^{-1}, colour shading) valid at 1500 UTC on 3 March 2008 in the following experiments: (a) CTRL, (b) NoCH-D36, and (c) NoF-D36. The sea ice edge is shown by a thick white curve. The red capital letters PL show the approximate central position of the simulated polar low.

most likely played a crucial indirect role in supporting an environment favourable for the PL development. The individual roles of sensible and latent heat fluxes for polar low developments have not often been addressed and will therefore be discussed in the subsection below.

4.2.2. Sensible or latent heat fluxes

Firstly, we will analyse the effect of turning off sensible or latent heat fluxes throughout the whole simulations. At 1200 UTC on 3 March, the removal of surface sensible heat fluxes resulted in a 2 hPa weaker PL (72°N, 8°E), and it was simulated about 2° farther east as compared to the CTRL run (Figure 9(a) vs. 2(a), respectively). Only latent heat fluxes (NoLHF), on the other hand, resulted in a 3 hPa weaker PL (72.5° N, 5°E) than what was seen in the CTRL, and the PL was simulated about 1° too far southeast (Figure 10(a) vs. 2(a), respectively). West of the PL, both the NoSHF and NoLHF showed weaker pressure gradients as compared to the CTRL, which explains the about 2–6 m s^{-1} lower maximum surface wind speed seen west of the PL. Based on the discussion above, we suggest that the individual effect of sensible or latent fluxes played a modest role in setting up the initial stage of the PL.

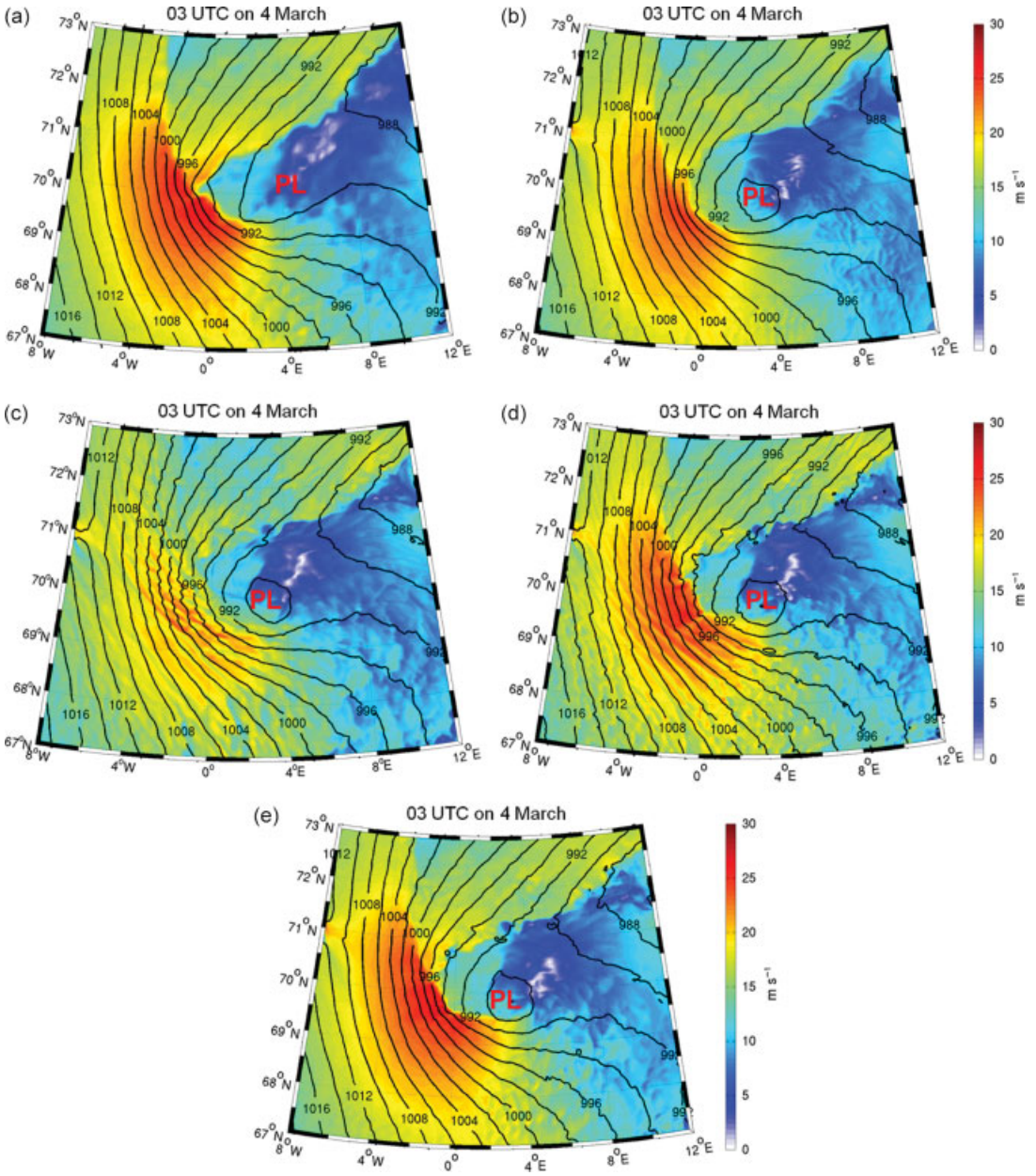

Figure 8. Mean-sea-level pressure (MSLP, hPa, black contours) and surface wind speed (m s^{-1}, colour shading) valid at 0300 UTC on 4 March 2008 in the following experiments: (a) CTRL, (b) NoCH-D48, (c) NoF-D48, (d) NoSHF-D48, and (e) NoLHF-D48. The red capital letters PL show the approximate central position of the simulated polar low.

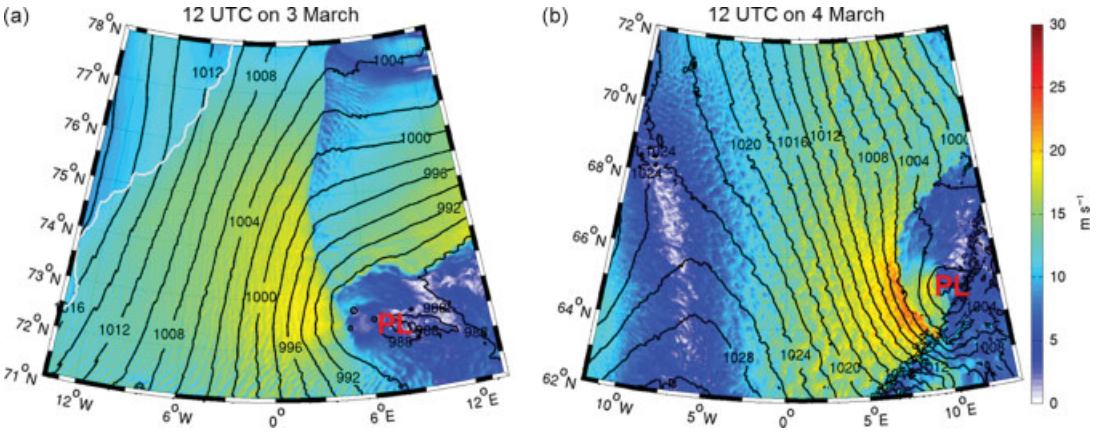

Figure 9. Mean-sea-level pressure (MSLP, hPa, black contours) and surface wind speed (m s^{-1}, colour shading) in the NoSHF experiment for the following times: (a) 1200 UTC on 3 March, and (b) 1200 UTC on 4 March, 2008. The sea ice edge is shown by a thick white curve. The red capital letters PL show the approximate central position of the simulated polar low.

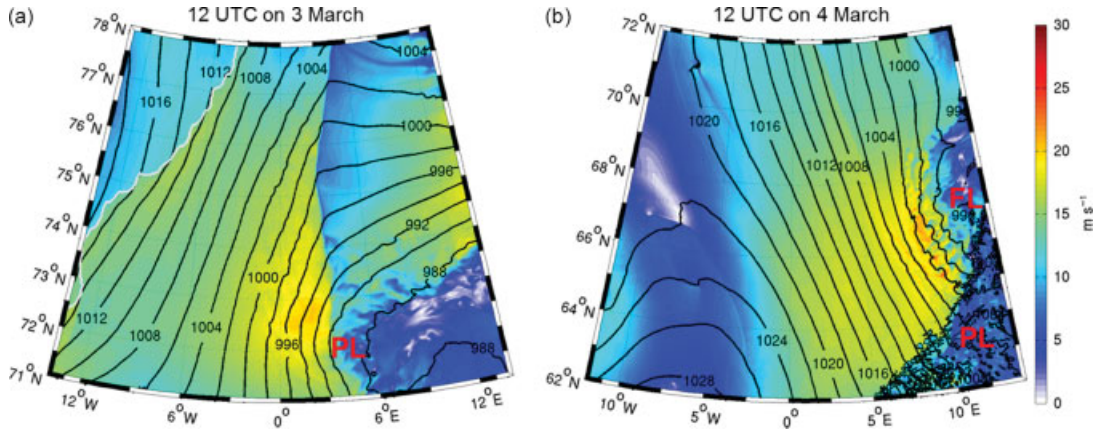

Figure 10. Mean-sea-level pressure (MSLP, hPa, black contours) and surface wind speed (m s^{-1}, colour shading) in the NoLHF experiment for the following times: (a) 1200 UTC on 3 March, and (b) 1200 UTC on 4 March, 2008. The sea ice edge is shown by a thick white curve. The red capital letters PL and FL show the approximate central position of the simulated polar low and the 'false low', respectively.

As the PL matured, sensible heat fluxes became gradually more important in that a reduction in PL intensity from 4 to 8 hPa was seen (Table 2). The NoLHF, however, showed that latent heat fluxes became crucial for the PL as it matured in that it weakened by 5 to 9 hPa (Table 2) and died away at 0900 UTC on 4 March. Figure 9(b) shows that at 1200 UTC on 4 March, the NoSHF simulated a 1001 hPa deep PL that was seen about 2° further south relative to the CTRL (Figure 2(d)). The weaker intensity (6 hPa) most likely explains the approximately 5 m s^{-1} lower maximum surface wind speed west of the PL. In Figure 10(b), the remnant of the PL (1006 hPa) in the NoLHF made landfall (64°N, 11°E) about 6 hours too early as compared to the CTRL (Figure 2(d)), which shows that the absence of latent heat fluxes caused the PL to move faster southeastward as it matured. A 'false' low (FL), which was initiated 4° further east of the PL at about 1500 UTC on 3 March (not shown), made landfall several hundred km further north at 67°N, 14°E (Figure 10(b)).

Based on the NoF-D48 it should not be surprising that the NoSHF-D48 and NoLHF-D48 showed a minor direct role of sensible and latent heat fluxes, respectively. At 0300 UTC on 4 March, the NoSHF-D48 (Figure 8(d)) and the NoLHF-D48 (Figure 8(e)) showed similar intensity as seen in the CTRL (Figure 8(a)), which implies that sensible and latent heat fluxes did not have a direct effect on the mature PL. However, as compared to the CTRL, the slightly weaker pressure gradients and reduction in maximum surface wind speed (2–5 m s^{-1}) in both experiments (NoSHF and NoLHF) suggest that sensible and latent heat fluxes had a minor direct effect on the PL intensity. As the PL matured, both types of surface flux played a modest indirect role in that only a 1–3 hPa weaker PL was simulated (Table 2).

During a 'hurricane-like' polar low development over the Barents Sea in 2002, similar experiments to those carried out in the present study suggested a dominant role of sensible heat fluxes as the polar low matured, while latent heat fluxes played a modest role. Since deep baroclinicity is not largely affected by surface energy flux modifications, the Barents Sea polar low was not sensitive to surface energy flux modifications until the baroclinicity weakened as it matured. However, as will be shown below, during the PL development the low-level baroclinic environment was affected by surface energy flux and condensational heating modifications, which in turn affected the PL intensity throughout its whole life cycle. The above discussion shows that the individual effect of each surface energy flux (sensible or latent heat) may be different to their combined effect, and that this may also be different from case to case for polar lows.

4.3. *Interpretation of the sensitivity experiments*

This subsection attempts to demonstrate the indirect effect the various physical processes had on the low-level baroclinic environment as well as the thermal structure of the PL and distribution of convection. This was done by comparing the 700–1000 hPa thickness, vertical velocity at 850 hPa, and potential temperature at 920 hPa between the CTRL and the NoCH-D36, NoF-D36, NoSHF and NoLHF experiments. The comparison was obtained by constructing plots at 0300 UTC on 4 March, i.e. at a time when the experiments showed large deviations in minimum MSLP relative to the CTRL run (Table 2), and during a time that the PL should have undergone baroclinic forcing (Figure 3(c)–(d)).

The absence of condensational heating (NoCH-D36) resulted in a 2 hPa weaker PL, which was simulated around 1° further to the southeast as compared to the CTRL (Figure 11(b) vs. 11(a), respectively). The 920 hPa potential temperature and the 700–1000 hPa thickness at the PL central area were approximately 2 K colder and 20 m lower, respectively. The warm tongue seen in the CTRL was slightly colder (274 K) and smaller and had advected further southeast, stretching from about 68.5° N, 2°E northeastward on the PL's western side. This suggests that slightly weaker baroclinic instability in the NoCH-D36, which may explain the 2 hPa weaker PL. This also implies that condensational heating to some extent warmed and maintained the baroclinic structure of the warm tongue (i.e. Figure 11(b)). The small differences in the baroclinic environment between the NoCH-D36 and the CTRL lasted until the PL made landfall (not shown), which could explain their relatively small difference in PL intensity with time (Table 2). How the variability in the simulated moist convection (i.e. vertical velocity) between the NoCH-D36 and the CTRL (i.e. Figure 11(b) vs. 11(a), respectively) affects the PL intensity was difficult to answer and will not be further discussed. It should be mentioned that in the NoCH, the warm tongue discussed above was largely smoothed out (not shown) and much colder at the initial stage of the PL. As the PL matured in the NoCH, the weaker baroclinicity was

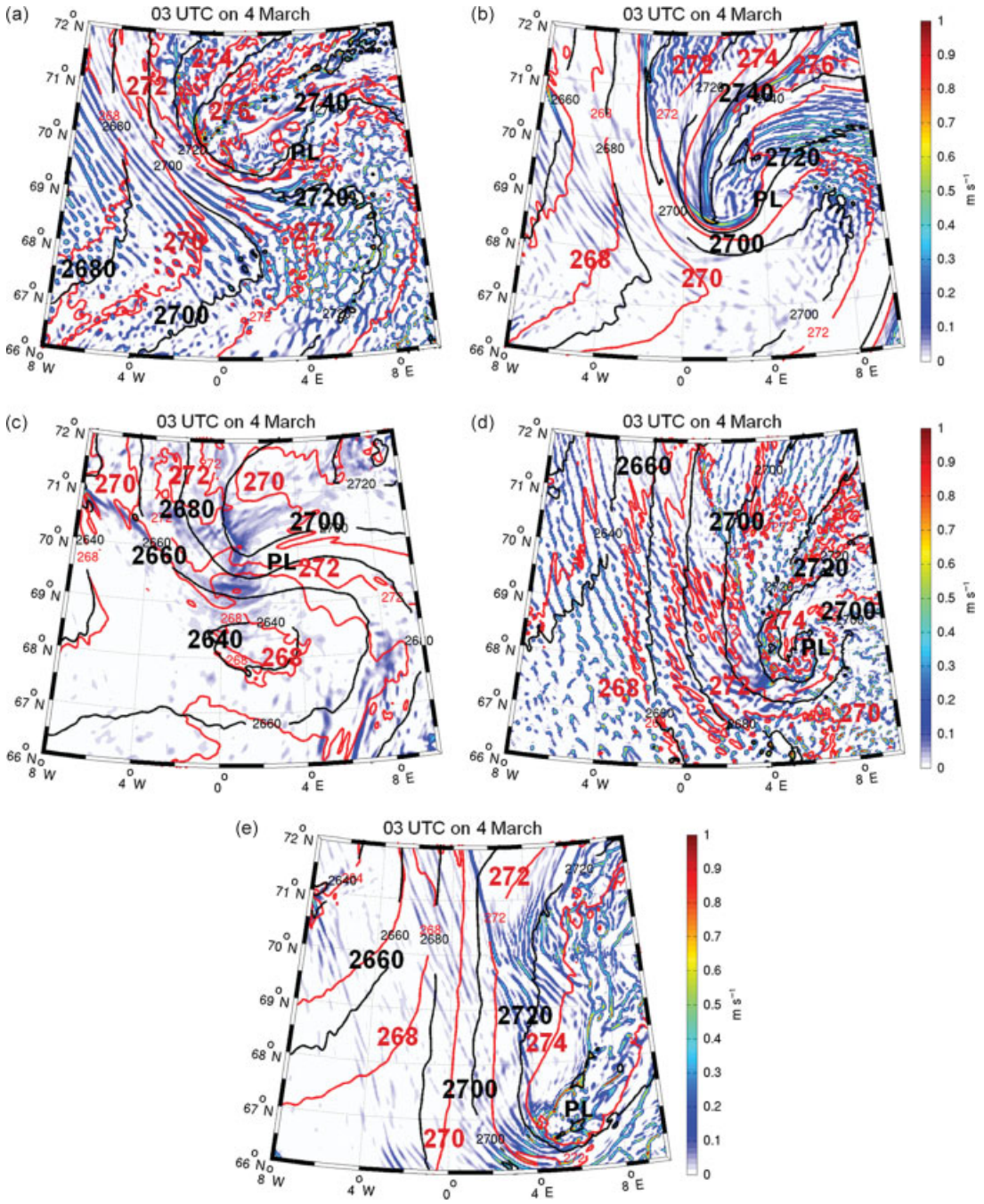

Figure 11. Vertical wind speed (m s^{-1}, colour shading) at 850 hPa surface, potential temperature at 920 hPa (K, red contours) and 700–1000 hPa thickness (20 m interval, black contours) at 0300 UTC on 4 March in the following experiments: (a) CTRL, (b) NoCH-D36, (c) NoF-D36, (d) NoSHF, and (e) NoLHF. The black capital letters (PL) show the approximate central position of the simulated polar low at the surface levels in each experiment.

consumed (not shown), which most likely resulted in the dramatic reduction in the PL intensity (NoCH vs. CTRL, Table 2). However, in the NoCH, the surface energy fluxes were about 20–40% lower because of lower surface wind speed, which in turn could have also contributed to the weakening of the PL.

Now let us look at the indirect role of surface energy (sensible and latent heat) fluxes for the PL intensity. The absence of surface energy fluxes (NoF-D36) resulted in a 6 hPa weaker PL as compared to the CTRL (Table 2), but the PL positions were similar (Figure 11(c) vs. 11(a), respectively). The overall 920 hPa potential temperature and 700–1000 hPa thickness were around 2–4 K and 20–60 m lower, respectively. Further, the warm tongue so clearly evident in the CTRL was smoothed out, which was most likely caused by the much weaker convection in this area (Figure 11(c) vs. 11(a), respectively). This would certainly have a negative effect on the baroclinic forcing on the PL, which in turn could explain the drastic reduction in the PL intensity and finally its death (i.e. NoF-D36, Table 2). Thus, surface energy fluxes seem to be essential in order to maintain the baroclinic environment favourable for the PL development, after the initial baroclinic environment had been set up. The absence of surface fluxes (NoF-D36) resulted in modest moist convection throughout the whole simulation, as demonstrated by the weak vertical velocities seen in Figure 11(c). As a result, less low-level convergence took place (not shown), which certainly would have a

negative effect on the PL intensity. However, it is difficult to address the magnitude of moist convection and the PL thermal structure for the intensity of the PL development in the NoF-D36 run.

Let us now look at the indirect role of only sensible heat fluxes. The NoSHF reproduced a 2 hPa weaker PL, which was simulated around 1° further to the southeast as compared to the CTRL (Figure 11(d) vs. 11(a), respectively). The potential temperature (272 K) curving northward along the PL central structure showed that the 4 K colder tongue had wrapped around the PL on its southern side, in good agreement with the 700–1000 hPa thickness (2720 m). The above observations suggest that by turning off sensible heat fluxes, a larger part of the baroclinicity was consumed as the PL moved faster southeastward into a warmer and less baroclinic environment, which was in agreement with the evolution of the baroclinicity in the CTRL (Figure 3(c)–(d)). The NoSHF showed relatively strong convection at the central area of the PL as compared to the CTRL (Figure 11(d) vs. 11(a), respectively), which implies that moisture fluxes (i.e. latent heat fluxes) and hence condensational heating could explain the relatively intense PL (Table 2) after the weaker baroclinicity was consumed (not shown). It should be mentioned that maximum latent heat fluxes seen southwest of the PL in the NoSHF were about 10–20% lower during the PL lifetime as compared to the CTRL (not shown) because of weaker surface wind speed (i.e. Figure 6(c)–(d)), which minimized the positive feedback on the PL intensity of moist convection and condensational heating.

The absence of only latent heat fluxes resulted in the PL being weakened by 7 hPa and being seen around 3° further southeast as compared to the CTRL (Figure 11(e) vs. 11(a), respectively). As the PL had moved into a warmer and less baroclinic environment, the 920 hPa potential temperature and 700–1000 hPa thickness at the central area of the PL were rather unchanged, showing 2 K and 20 m lower values, respectively. Plots of previous times (not shown) showed that the initial baroclinic structure of the warm tongue discussed above was smoothed out by the absence of latent heat fluxes (NoLHF), which in turn weakened the baroclinic forcing, in agreement with the evolution of the PL in the NoCH discussed above. The above observations suggest that latent heat fluxes were essential to set up and maintain the baroclinic environment favourable for the PL development. As the weaker baroclinicity was consumed, the reduced organized convection in the NoLHF (Figure 11(e) vs. 11(a), respectively) was not strong enough to sustain the PL development, and thus the PL died away. However, it is difficult to address the magnitude of moist convection and the PL thermal structure for the intensity of the development in the NoLHF. It should be mentioned that sensible heat fluxes seen southwest of the PL in the NoLHF during the cyclogenesis stage were about 20–30% lower as compared to the CTRL (not shown), which minimized the positive feedback on the PL intensity of sensible heat fluxes.

The above observations demonstrate that it is not trivial to compare the PL intensity in the CTRL hour by hour with each experiment listed in Table 2, since the PL intensity seemed to depend on the baroclinic nature of the PL environment, the maturity of the baroclinic instability, which in turn was dependent on the southeastward speed of the PL, and the variability in the simulated moist convection, thermal structure of the PL core, and surface energy fluxes in some of the experiments.

5. Summary and discussions

In this study, high-resolution (3 km mesh) WRF simulations were used to analyse the underlying physics of a polar low (PL) that was observed by three research aircraft missions (section 1) during the IPY-THORPEX campaign. The full-physics simulation (CTRL) reproduced maximum surface wind speed, intensity, and PL track quite well according to dropsonde observations and satellite images. The PL (986 hPa) developed in a low-level (750–1000 hPa) baroclinic environment at the intersection of two well-defined convergence zones, with maximum surface wind speed on its cold western side of about 25 m s^{-1}. This resulted in maximum surface sensible and latent heat fluxes of approximately 320 W m^{-2} and 250 W m^{-2}, respectively. As the PL moved southeastward into a warmer and less baroclinic environment it weakened by 10 hPa (996 hPa), but because of increased pressure gradients on its southwestern side, a maximum surface wind of about 27 m s^{-1} was seen. The maximum sensible and latent heat fluxes increased to 450 W m^{-2} and 400 W m^{-2}, respectively. Similar to dropsonde observations, the simulated PL developed a warm core that was about 4°C warmer than the air to its west.

To reveal the underlying physics of the PL, two types of sensitivity experiments were designed. First, an ordinary sensitivity experiment was carried out, in which physical processes such as condensational heating and sensible and/or latent heat fluxes were turned off throughout the whole integration time. A second type of experiment (delayed) was designed in which the physical processes were turned off at later times. In these latter experiments, it is easier to analyse whether the absence of a physical process directly affected the PL itself or indirectly through modification of the surrounding PL environment over time.

The ordinary experiments showed, as several other studies with similar experiments have shown, that in the absence of energy supply from the ocean (sensible and latent heat fluxes) the polar low did not develop. Evidence was found that the model failed to simulate the initial baroclinic structure (i.e. the two convergence zones) of the PL development, and thus the PL did not develop. Further, the ordinary experiments revealed that latent heat fluxes, and to a large extent condensational heating, played a crucial role for the PL intensity as it matured. Only sensible heat fluxes, on the other hand, played a moderate role for the PL intensity.

However, based on both type of sensitivity experiments we believe that low-level baroclinic energy conversion dominated the PL development, while other physical processes had a minor direct impact on the PL intensity. We rather find that latent heat fluxes, and to some extent sensible heat fluxes, played an important indirect role in setting up the low-level baroclinic environment favourable for the PL development. As the PL matured, latent heat fluxes played a crucial indirect role for the PL intensity in that it was essential to maintain a low-level baroclinic environment supportive for the PL development, while sensible heat fluxes played a minor role. Condensational heating, on the other hand, was essential to set up the initial low-level baroclinic environment, while it had a smaller indirect effect in maintaining the low-level baroclinic environment thereafter. The experiments did indicate that in late mature stage, after baroclinicity vanished, surface energy (sensible and/or latent heat) fluxes might have contributed directly

to the PL energetic. However, it was difficult to separate the role of surface energy fluxes and condensational heating in the late mature stage using the present experiments.

We found evidence that the absence of the physical processes over time, especially latent heat fluxes and condensational heating, resulted in a faster consumption of the modified low-level baroclinic energy, which could partly explain the strong reduction in PL intensity with increasing time between the sensitivity experiments and the CTRL run. However, we do not have sufficient evidence to support this explanation. Furthermore, how the variability in the simulated convection, thermal structure of the PL central structure, and surface energy fluxes in some of the experiments affected the PL intensity was difficult to answer.

As demonstrated above, it is not trivial to analyse sensitivity experiments, because of the complex interplay of a variety of physical processes in each experiment. However, as this article shows, the new types (delayed) of sensitivity experiment lead to different suggestions on how the various physical processes affected the PL development as compared to the ordinary experiments. We therefore strongly recommend other authors to carry out similar delayed (D) experiments in future polar low studies. For future research, physical processes could be turned off for a short time period to analyse the potential reduction and intensification as they are off–on. It should also be mentioned that the absence of any physical process over a long time period could have led to different interactions between the PL and the upper-level PV anomaly in each experiment, and thus differences in upper-level forcing, which could have affected the PL intensity. In order to shed light on the role of different upper and low-level interactions in each experiment, a PV inversion should be carried out for each experiment. However, upper-level PV forcing was not in the scope of this study and was thus not discussed in detail.

Acknowledgements

This study was supported by the Norwegian Research Council through the project 'THORPEX-IPY: Improved forecasting of adverse weather in the Arctic – present and future' (grant no. 175992). The authors are grateful to WRF-help in the configurations of sensitivity experiments and the set-up of the WRF model. In particular, the authors wish to thank Gunnar Wollan and Ole Widar Saastad for their support in the implementation of WRF at the University of Oslo. Special thanks go to 'metos-drift' for consistently fast answers and motivating support. The first author wishes particularly to thank Bjørn Egil Nygård and Øyvind Hodnebrog for their support with Matlab and WRF. Special thanks go to Gunnar Noer at the Norwegian Meteorological Institute for his valuable comments and to all our colleagues at MetOs for their motivating support and discussions.

References

Albright MD, Reed RJ, Ovens DW. 1995. Origin and structure of a numerically simulated polar low over Hudson Bay. *Tellus* **47A**: 834–848.

Bresch JF, Reed RJ, Albright MD. 1997. A polar-low development over the Bering Sea: Analysis, numerical simulation, and sensitivity experiments. *Mon. Weather Rev.* **105**: 3109–3130.

Chen F, Dudhia J. 2001. Coupling an advanced land surface–hydrology model with the Penn State–NCAR MM5 modeling system. Part I: Model implementation and sensitivity. *Mon. Weather Rev.* **129**: 569–585.

Claud C, Heinemann G, Raustein E, McMurdie L. 2004. Polar low *le Cygne*: Satellite observations and numerical simulations. *Q. J. R. Meteorol. Soc.* **130**: 1075–1102.

Craig GC, Gray SL. 1996. CISK or WISHE as the mechanism for tropical cyclone intensification. *J. Atmos. Sci.* **53**: 3528–3540.

Dudhia J. 1989. Numerical study of convection observed during the Winter Monsoon Experiment using a mesoscale two-dimensional model. *J. Atmos. Sci.* **46**: 3077–3107.

Føre I, Kristjánsson JE, Sætra Ø, Breivik Ø, Røsting B, Shapiro M. 2011. The full life cycle of a polar low over the Norwegian Sea observed by three research aircraft flights. *Q. J. R. Meteorol. Soc.* **137**: 1659–1673.

Føre I, Kristjánsson JE, Kolstad EW, Bracegirdle TJ, Sætra Ø, Røsting B. 2012. A 'hurricane-like' polar low fuelled by sensible heat flux: High-resolution numerical simulations. *Q. J. R. Meteorol. Soc.* DOI: 10.1002/qj.1876.

Hong S-Y, Noh Y, Dudhia J. 2006. A new vertical diffusion package with an explicit treatment of entrainment processes. *Mon. Weather Rev.* **134**: 2318–2341.

Hoskins BJ, McIntyre ME, Robertson AW. 1985. On the use and significance of isentropic potential vorticity maps. *Q. J. R. Meteorol. Soc.* **111**: 877–946.

Irvine EA, Gray SL, Methven J. 2011. Targeted observations of a polar low in the Norwegian Sea. *Q. J. R. Meteorol. Soc.* **137**: 1688–1699.

Janjić ZI. 1994. The step-mountain eta coordinate model: Further developments of the convection, viscous sublayer, and turbulence closure schemes. *Mon. Weather Rev.* **122**: 927–945.

Janjić ZI. 2000. Comments on 'Development and evaluation of a convection scheme for use in climate models'. *J. Atmos. Sci.* **57**: 3686.

Kolstad EW. 2006. A new climatology of favourable conditions for reverse-shear polar lows. *Tellus* **58A:**: 344–354.

Kolstad EW, Bracegirdle TJ. 2008. Marine cold-air outbreaks in the future: An assessment of IPCC AR4 model results for the Northern Hemisphere. *Clim. Dyn.* **30**: 871–885.

Kristjánsson JE, Barstad I, Aspelien T, Føre I, Godøy Ø, Hov Ø, Irvine E, Iversen T, Kolstad E, Nordeng TE, McInnes H, Randriamampianina R, Reuder J, Sætra Ø, Shapiro M, Spengler T, Ólafsson H. 2011. The Norwegian IPY-THORPEX: Polar lows and Arctic fronts during the 2008 Andøya campaign. *Bull. Am. Meteorol. Soc.* **92**: 1443–1466.

McInnes H, Kristiansen J, Kristjánsson JE, Schyberg H. 2011. The role of horizontal resolution for polar low simulations. *Q. J. R. Meteorol. Soc.* **137**: 1674–1687.

Mailhot J, Hanley D, Bilodeau B, Hertzman O. 1996. A numerical case study of a polar low in the Labrador Sea. *Tellus* **48A**: 383–402.

Mlawer EJ, Taubman SJ, Brown PD, Iacono MJ, Clough SA. 1997. Radiative transfer for inhomogeneous atmosphere: RRTM, a validated correlated-k model for the longwave. *J. Geophys. Res.* **102**: 16663–16682.

Montgomery MT, Farrell BF. 1992. Polar low dynamics. *J. Atmos. Sci.* **49**: 2484–2505.

Nordeng TE. 1987. The effect of vertical and slantwise convection on the simulation of polar lows. *Tellus* **39A**: 354–375.

Rasmussen EA, Turner J (eds). 2003. *Polar Lows*. Cambridge University Press: Cambridge.

Renfrew IA, Moore GWK, Guest PS, Bumke K. 2002. A comparison of surface layer and surface turbulent flux observations over the Labrador Sea with ECMWF analyses and NCEP reanalyses. *J. Phys. Oceanogr.* **32**: 383–400.

Sardie JM, Warner TT. 1985. A numerical study of the development mechanisms of polar lows. *Tellus* **37A**: 460–477.

Skamarock WC, Klemp JB, Dudhia J, Gill DO, Barker DM, Wang W, Powers JG. 2005. *'A description of the Advanced Research WRF version 2.'* NCAR Technical Note TN-468+STR, 88 pp. NCAR: Boulder, CO.

Thompson G, Rasmussen RM, Manning K. 2004. Explicit forecasts of winter precipitation using an improved bulk microphysics scheme. Part I: Description and sensitivity analysis. *Mon. Weather Rev.* **132**: 519–542.

Thompson G, Field PR, Hall WD, Rasmussen RM. 2006. 'A new bulk microphysical parameterization for WRF (& MM5).' Paper 5.3, pp 1–11 in *Proceedings of the 7th Weather Research and Forecasting Model Workshop*. NCAR Mesoscale and Microscale Meteorology Division: Boulder, Colorado, USA. http://www.mmm.ucar.edu/wrf/users/workshops/

Undén P, Rontu L, Järvinen H, Lynch P, Calvo J, Cats G, Cuxart J, Eerola K, Fortelius C, Garcia-Moya JA, Jones C, Lenderlink G, McDonald A, McGrath R, Navascues B, Nielsen NW, Ødegaard V, Rodriguez E, Rummukainen M, Room R, Sattler K, Sass BH,

Savijärvi H, Schreur BW, Sigg R, The H, Tijm A. 2002. '*HIRLAM-5 scientific documentation.*' HIRLAM-5 Project, c/o Per Undén, SMHI, S-601 76 Norrköping, Sweden, 144 pp.

Wu LT, Petty GW. 2010. Intercomparison of bulk microphysics schemes in model simulations of polar lows. *Mon. Weather Rev.* **138**: 2211–2228.

Wu LT, Martin JE, Petty GW. 2011. Piecewise potential vorticity diagnosis of the development of a polar low over the Sea of Japan. *Tellus* **63A**: 198–211.

Yanase W, Fu G, Niino H, Kato T. 2004. A polar low over the Japan Sea on 21 January 1997. Part II: A numerical study. *Mon. Weather Rev.* **132**: 1552–1574.

